Defects in Amorphous Semiconductors: The Case of Amorphous Indium Gallium Zinc Oxide

A. de Jamblinne de Meux,[1,2] G. Pourtois,[2,3] J. Genoe,[1,2] and P. Heremans[1,2]
[1]*KU Leuven, ESAT, B-3001 Leuven, Belgium*
[2]*IMEC, Kapeldreef 75, B-3001 Leuven, Belgium*
[3]*Plasmant Research Group, Department of Chemistry, University of Antwerp, 2610 Wilrijk-Antwerp, Belgium*

(Received 27 November 2017; revised manuscript received 9 March 2018; published 25 May 2018)

Based on a rational classification of defects in amorphous materials, we propose a simplified model to describe intrinsic defects and hydrogen impurities in amorphous indium gallium zinc oxide (*a*-IGZO). The proposed approach consists of organizing defects into two categories: point defects, generating structural anomalies such as metal—metal or oxygen—oxygen bonds, and defects emerging from changes in the material stoichiometry, such as vacancies and interstitial atoms. Based on first-principles simulations, it is argued that the defects originating from the second group always act as perfect donors or perfect acceptors. This classification simplifies and rationalizes the nature of defects in amorphous phases. In *a*-IGZO, the most important point defects are metal—metal bonds (or small metal clusters) and peroxides (O—O single bonds). Electrons are captured by metal—metal bonds and released by the formation of peroxides. The presence of hydrogen can lead to two additional types of defects: metal-hydrogen defects, acting as acceptors, and oxygen-hydrogen defects, acting as donors. The impact of these defects is linked to different instabilities observed in *a*-IGZO. Specifically, the diffusion of hydrogen and oxygen is connected to positive- and negative-bias stresses, while negative-bias illumination stress originates from the formation of peroxides.

DOI: 10.1103/PhysRevApplied.9.054039

I. INTRODUCTION

Amorphous indium gallium zinc oxide (*a*-IGZO) is a semiconductor used in thin-film transistors (TFTs) for large-area applications. This material is making its entry into the display industry thanks to its improved performance compared to amorphous silicon [1] in terms of mobility ($>10\ \mathrm{cm^2/V\,s}$), low *off* current, and stability [2,3]. Despite its benefits, a recurrent problem with *a*-IGZO TFTs lies in the shift of the transfer curve (drain-source current vs gate voltage) upon the application of prolonged gate-bias stresses. Three cases are usually distinguished: negative-bias stress (NBS), negative-bias illumination stress (NBIS), and positive-bias stress (PBS) [4,5]. NBS and NBIS instabilities shift the transfer curve of the TFT negatively, while PBS shifts it positively. Both NBS and PBS recover upon rest after stress, while NBIS does not [6–11].

The fundamental understanding of *a*-IGZO and the origin of its bias instabilities are still controversial due to the complexity of the amorphous nature of the material. For instance, the origin of PBS has been explained by a great many possible mechanisms: charge trapping processes occurring at the interfaces and/or in the dielectric [12,13], the creation of deep traps [12–14] in the semiconductor, the absorption of oxygen or water molecules at the channel interface [12,13,15], the removal of oxygen interstitials [15], the creation of undercoordinated cation pairs [16], the capture of electrons by oxygen vacancies [17], the reduction of peroxide concentration [18], and the diffusion of hydrogen [19,20].

Similarly, the NBS instability has been explained by several possible mechanisms, namely, by charge trapping occurring at the dielectric interface [13,21], by positively charged oxygen vacancies [13,21,22], and by the diffusion of oxygen [23]. Finally, several causes have also been proposed for NBIS: charge trapping in the dielectric [12,13,24], driven by the ionization of oxygen vacancies [10,17,21,25–28], trapping by zinc interstitials, and the formation of a hydrogen-related complexes [13], desorption of oxygen molecules or moisture [12,13], desorption of hydrogen [29], formation of oxygen interstitials [10,15], diffusion of hydrogen and charge trapping at the interfaces [30], formation of peroxides [31], and, finally, trapping of electrons in hydrogen bistable states [32].

In typical crystalline semiconductors, doping as well as electronic instabilities are explained by the presence of defects. Crystals are perfectly ordered phases and deviations from this order lead to point defects with an electronic signature in the gap. These electronic states dope or trap charges in the material by capturing or providing electrons (holes) to the conduction band (valence band). As, in an amorphous phase, the same mechanisms are expected to take place, defects in disordered materials are studied similarly to defects in crystalline materials. In this article,

we show that this approach is misleading and complicates the understanding of defects in *a*-IGZO. Currently, oxygen vacancies and oxygen interstitials are the most investigated defects in *a*-IGZO. They present particularly complex behaviors which are summarized below.

The most investigated defect in *a*-IGZO is the oxygen vacancy [17,23,25,33,34]. This defect is obtained by removing an oxygen atom from a stoichiometric model, which generally leads to the formation of a metal—metal bond (or a small metal cluster), which is often referred to as a "neutral oxygen vacancy" [17,23,25,33,34]. Upon ionization, this metal—metal (M—M) bond breaks. The resulting structure is then typically referred to as an "ionized oxygen vacancy." Although straightforward, these definitions are nevertheless rapidly confusing: oxygen vacancies in their neutral state do not always form metal—metal bonds [23]. In the absence of these M—M bonds, the local atomic structure of *a*-IGZO is similar to the one without a vacancy, but electrons are induced directly in the conduction band. The oddity is that no particular local variation can be observed: there is no new electronic state signature in the energy gap and no abnormal change in the local atomic structure [23]. The only changes are "global": the material has a total charge of $+2|e|$ per unit cell and, globally, one oxygen atom is missing. The combination of these factors shows that, in an amorphous material, most oxygen vacancies cannot simply be considered point defects in the sense known from crystalline materials. Also, if oxygen vacancies were point defects, one would expect that providing electrons to an "ionized vacancy" would turn it into a "neutral vacancy," i.e., a metal—metal bond. However, in amorphous IGZO, we show in this paper that the ionized vacancy is not neutralized by injected electrons, and no metal—metal bond forms. Instead, the vacancy remains "ionized" and the added electrons go to the conduction band. Furthermore, we observe that one may also generate such neutral vacancies (M—M bonds) by adding charges to a stoichiometric model [35], which is, at best, unexpected if we consider a M—M bond a neutral vacancy.

In a similar way, an "oxygen interstitial" is typically induced by adding an oxygen atom in a stoichiometric model. The added oxygen can then be bonded to an oxygen site to create a peroxide (an oxygen—oxygen single bond) [15,36]. However, a similar peroxide can also form spontaneously upon hole injection in a stoichiometric system [31,37]. Similar to the previous paragraph, if we link oxygen interstitials to peroxides, then an oxygen interstitial can be generated in a stoichiometric model upon hole injection, which is, again, surprising. While these definitions are not technically wrong, they may rapidly lead to confusion in the description of defect behavior.

The complex picture presented above can be greatly simplified by classifying the defects into two categories: (i) normal point defects inducing clear local variations in the amorphous structure, and (ii) "nonstoichiometric" defects, which affect the material only globally due to a reconstruction of the amorphous matrix. To support this classification, we present the properties of defects in *a*-IGZO using first-principles simulations based on a 5-nm-long model containing 490 atoms (with a $10.82 \times 10.75 \times 52.17$ Å unit cell) and a hybrid functional. We take care to use an elongated model to ensure that the first conduction band is localized in the elongated direction, as displayed in Fig. 1 and as discussed in Ref. [38]. This characteristic is expected to provide a more accurate description of defective *a*-IGZO than what was reported in previous studies, where the atomistic models were too small to display a proper localization of the wave functions [38] in the amorphous state.

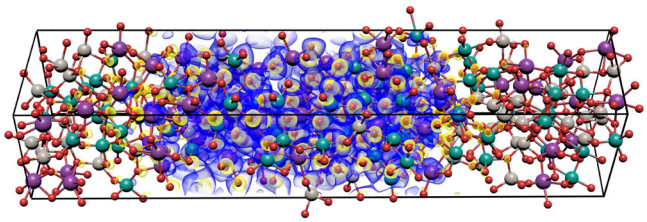

FIG. 1. Isosurface of the wave function computed for the first conduction band of an *a*-IGZO model containing 490 atoms. The unit cell has a physical dimension of $10.82 \times 10.75 \times 52.17$ Å. Thanks to the size of the model used, the wave function gets localized along the elongated direction. The color of the wave function represents its phase. Oxygen atoms are shown in red, indium in purple, zinc in gray, and gallium in green, the isovalue of the wave function is set to 0.005.

The method and theoretical challenges posed by the study of *a*-IGZO and, more generally, by high-mobility amorphous semiconductors are briefly discussed in the following section. We highlight that density-functional-theory (DFT) simulations in these materials should be interpreted with caution and that some approaches developed to study defective crystalline materials cannot be systematically transposed to the case of amorphous materials. We illustrate our point by focusing on the case of *a*-IGZO and propose a general formalism to describe the defects in these complex amorphous phases. We finally correlate our findings with the occurrence of various bias instabilities in *a*-IGZO and build a clarified picture of the fundamental electrical properties of this material.

II. METHODOLOGY

Two fundamental sources of inaccuracies exist in the modeling process of *a*-IGZO using standard DFT simulations. They find their roots in the dimensions of the atomistic model and in the exchange-correlation functional used. The most fundamental issue, which is common to any DFT calculation, arises from the approximations used to treat the exchange-correlation effects. They induce a large underestimation of the electronic gap of the materials and

tend to promote an artificial delocalization of the electrons. The problem is amplified in materials where electrons are strongly localized, as is the case in *a*-IGZO. Advanced treatments of the electronic exchange correlation, as available, for instance, in hybrid functionals, are hence needed to obtain a more realistic description of the electronic structure [39–41]. In our simulations, an improved description of the exchange correlation is obtained by a hybrid functional composed of 70% of the exchange-correlation energy obtained with the Perdew, Burke, and Ernzerhof (PBE) functional [42] combined with 30% of the exact Hartree-Fock exchange. The latter is built using a truncated Coulomb operator [43] and a cutoff of 5 Å within the auxiliary density-matrix methods [44] and a minimal auxiliary basis set.

The amount of HF exchange is increased to 30% to open the band gap to a value close to the experimental one, which is reported to range from 3.0 to 3.2 eV [45–47]. The resulting electronic band gap is 2.57 eV using the last tail state (last occupied state) as a measure of the valence-band energy. However, tail states may extend up to approximately 0.5 eV in the gap [48], hence leading to an artificial reduction of the computed band gap. Accounting for this effect, and based on the density of states reported in Fig. 2, the band gap can be estimated at about 2.9 eV.

The simulations are performed with the CP2K package [49,50]. All Brillouin-zone integrations are approximated with their values in Γ. Goedecker-Teter-Hutter pseudopotentials [51–53] are used to model core electrons, and the wave functions are expanded using a double ζ valence polarized molecular optimized (MOLOPT) atomic basis [54]. In all of the simulations, a plane-wave cutoff of 900 Ry is used with six grids and a relative cutoff of 60 Ry. The amorphous-IGZO model, shown in Fig. 1, contains 490 atoms within an elongated unit cell with the dimensions $10.82 \times 10.75 \times 52.17$ Å. It is generated with a method similar to the seed and coordinate algorithm [55] using the PBE functional for the initial relaxations. The resulting geometries are subsequently relaxed with the hybrid exchange-correlation functional for which all of the subsequent simulations are performed. Barriers between defect conformations are evaluated using a nudged elastic band (NEB) algorithm [56] combined with a spring constant of 0.05 atomic unit and a sampling of ten images. Because of the computational burden of the simulations (fully performed with the hybrid functional), a limited number of defect conformations are generated: four models of oxygen vacancies, one peroxide formed by the injection of holes, three formed by the addition of an oxygen atom, one *M*-H defect, and six O-H defects. These models are further defined with different charge states to analyze their stability with respect to the position of the Fermi level.

The dimensions of the atomic model are the second source of inaccuracies for the modeling of amorphous phases. Typically, DFT simulations of condensed phases are performed within periodic boundaries. While, for crystals, this approach is accurate due to their symmetry of translation, they are incompatible with amorphous materials. With state-of-the-art techniques, it is hardly possible to simulate a realistic amorphous film with billions of atoms. Therefore, these materials are commonly approximated by periodically repeating a disordered periodic unit cell. The chosen dimensions of the unit cell can strongly affect the modeling results. For large enough cells, periodic interactions are negligible and the model is considered accurate [38]. Owing to its high mobility [46], the conduction-band (CB) states of *a*-IGZO are unusually strongly delocalized compared to other amorphous materials, as they span over a few nanometers [38]. In any case, the dimensions of the model that has been used to describe *a*-IGZO is on the order of only about 10 Å [17,23,25,33,34] significantly smaller than the delocalization length of the CB. When the model dimension is smaller than the delocalization length, the CB is observed to be delocalized over the unit cell and, by the periodicity implied in the method, the delocalization is artificially extended to the entire material.

An additional challenge resides in the interpretation of the DFT results and their comparison to experimental observations. Indeed, the study of defects in crystalline semiconductors is based mainly on the extraction of their formation energies, which reflects their thermodynamic stability. The position of the defect charge transition levels indicates whether the defect is a deep or shallow donor or an acceptor. Interestingly, even in the crystalline phase, the evaluation of these parameters is not a straightforward task [57,58]. The main issues are similar to those discussed previously for the amorphous system, with the need to (i) account for an accurate treatment of the exchange-correlation functional, and (ii) to use models with unit cells (or a supercell) large enough to avoid interactions between the induced defects. It is also important to highlight that the energy levels obtained directly from electronic structure calculations (the Kohn-Sham energy levels) are not directly observable experimentally. The energy position of these energy levels may also differ, depending on the experimental technique used [57,58]. For instance, optical and electrical measurements may not agree due to the difference in the excitation time used to characterize the system. While an optical excitation is typically fast enough to prevent atomic relaxation processes, an electronic excitation is not. As a structural relaxation may substantially alter the energy levels obtained experimentally, defects may end up having a different signature in the band gap, depending on the way they are measured.

In *a*-IGZO, the computation of the charge transition levels is often problematic. Indeed, while these transition levels provide information on the position of the Fermi level at which an electron is captured or released by a defect, they also rely on the assumption that the defect creates a stable energy level in the energy gap. In the presence of such an

energy state, the defect can modify its conformation to accommodate the charges added or removed from this localized state, hence modulating its formation energy and the position of the associated Kohn-Sham energy level. The Fermi level (E_f) at which two charge states have the same energy (which depends on E_f) provides the transition level [57,58]. In *a*-IGZO, many defects do not create any states in the gap [15,23,31,36,37]. It hence results that whenever electrons are injected into or removed from these simulations, they are added or extracted from either the valence or the conduction band, and not from the defect itself. The resulting transition levels hence lose their original meaning [23]. This mechanism also reveals that the doping mechanism in *a*-IGZO is very different than the one in crystalline materials. In the latter, doping is thermally activated. For instance, electrons are provided to the conduction band by thermal excitation of electrons in defective states close to the conduction band. In *a*-IGZO, the absence of such defective states forbids this doping mechanism. Instead, donor defects directly provide electrons to the conduction band upon their formation and recapture them upon their dissolution.

III. DEFECTS IN AMORPHOUS *a*-IGZO

A defect is an abnormal variation with respect to a reference. For an amorphous structure, this reference is a "perfect" stoichiometric structure. However, the meaning of *perfect* is not unique in an amorphous phase. Indeed, the structure is defined only locally, by average bond lengths and coordination numbers. These characteristics are also quite permissive, with different distributions of acceptable bond lengths and coordination numbers [45,59–61]. The average coordination of indium in *a*-IGZO, for instance, varies from 4.8 to 5.6, depending on the sample preparation method. A non-negligible part of the indium can hence be coordinated four, five, or six times in a perfect stoichiometric amorphous structure [61], making the identification of a missing neighbor, e.g., a vacancy, difficult.

In order to simplify and offer a consistent model of defects in amorphous semiconductors, we propose to classify defects in these disordered phases in two categories. The first type of defects are "point defects" and are defined in a similar way to a crystalline material. More specifically, they represent an abnormal and local change in the atomic and electronic structure. In this framework, a variation is local whenever it is clearly localized in a space that is (much) smaller than the dimension of the model used and is abnormal if the resulting local variation can be clearly distinguished from the signature of any other part of the model.

The second type of defects are nonstoichiometric defects. These defects are simply defined as any defect changing the material stoichiometry. In an ionic material, such variations usually break the anion-cation balance, resulting in a spontaneous charging, and hence to doping. Although their doping effect may trigger the formation of point defects, we argue that the two types of defects are independent. Because the coordination number of each atom is not strictly fixed, the effect of the removal (or addition) of an atom in an amorphous structure can be averaged out throughout the structure. This averaging results in a charged structure presenting no well-defined point defects. As it is desirable to link the resulting doping to a defect, it is convenient to introduce an alternative type of defect, i.e., the nonstoichiometric defects, to explain these situations.

Within this framework, an oxygen vacancy acts as a donor, while an added oxygen (oxygen interstitial) is an acceptor. Both are nonstoichiometric defects, as they result in a change in the material stoichiometry. An intuitive interpretation is that oxygen atoms act as anions capturing two electrons. Hence, upon its addition to the matrix, the oxygen atom tends to capture two electrons, acting as an acceptor. Upon removal of an oxygen atom, the previously captured electrons are released: this corresponds to the behavior of a donor.

The most important point defects are metal—metal bonds (or small metal clusters) and peroxides (oxygen—oxygen single bond). The metal—metal bonds have an acceptor character, whereas peroxides act as donors.

For the definition of impurities, the disorder of the phase is not a problem. Indeed, their presence is a clear and well-localized abnormality. Hydrogen, for instance, leads to two types of impurities: hydrogen—metal bonds, which act as acceptors, and hydrogen-oxygen defects, acting as donors.

Table I summarizes the main characteristics of the defects in *a*-IGZO. The remainder of this section explores these characteristics by first-principles calculation on an elongated model of *a*-IGZO. We show that all of the results obtained support the proposed classification scheme and simplify the interpretation of the results.

A. Metal-metal defects

Metal-metal defects are obtained by removing (or strongly displacing) an oxygen atom from a stoichiometric atomic model. In this situation, the metals around the removed oxygen can interact and bind, as illustrated in Fig. 3. The metal-metal defect forms a localized state in the gap which is positioned, in the present simulations, in the lower part of the band gap (see Fig. 2). As expected, the conduction band is empty, indicating that the two electrons provided by the oxygen vacancy are captured by the metal-metal defect. When the Fermi level is pushed in the lower half of the band gap (e.g., by the application of a negative gate voltage in a transistor structure), the two electrons can be removed from the occupied gap state and the defect is ionized (2+). In amorphous IGZO, this mechanism is accompanied by a large structural relaxation, as illustrated in Figs. 4(b) and 4(c). This relaxation cures the formed metal-metal defect: the electronic state in which

TABLE I. Overview of the defects discussed in this work with their classification and doping effect. The number of electrons captured or released by a single defect upon creation is provided in parentheses after the doping type. The stability of these defects is dependent on the localization of the Fermi level (E_f): the last column indicates the position of E_f where the defects are expected to be stable. See Table II and the text for additional details. All defects capture electrons (or holes) upon creation and release them upon their dissolution. Only the metal—metal bond creates a localized state in the gap, but the defect dissolves if it is ionized.

Type of defect	Name	Doping effect	Stable for E_f in
Stoichiometric defects	Oxygen vacancy (V_O)	Donor ($2e^-$)	Band gap and in the VB
	Oxygen interstitial (O_i)	Acceptor ($2e^-$)	Close and in the CB
Point defects	Peroxide (O—O)	Donor ($2e^-$)	Close and in the VB
	Metal—metal bond (M—M)	Acceptor ($2e^-$)	Deep in the CB
Impurities	Oxygen—hydrogen bond (O—H)	Donor ($1e^-$)	CB, gap, and in the VB
	Metal—hydrogen bond (M—H)	Acceptor ($1e^-$)	Deep in the CB

the metal—metal bond has trapped two electrons vanishes. Therefore, we cannot speak of a point defect anymore, as the structure has to reconstruct itself to average out the effect of a missing oxygen atom. Still, the total structure carries two positive charges because the global number of metals (having a positive charge) and oxygens (having a negative charge) are not in balance since there is one oxygen atom missing. We hence speak of a nonstoichiometric defect: the oxygen vacancy. This defect is a donor able to provide two electrons to the system upon formation. By contrast, the metal—metal bond is a point defect able to trap two electrons.

The reintroduction of electrons, e.g., by increase of the gate voltage, does not lead to the (re)formation of the metal-metal point defect. Indeed, there is no electronic trap level in the band gap able to capture electrons. Instead, the two electrons are simply delocalized in the conduction band, as shown in Fig. 5, such that the total structure is neutral in charge. Hence, the oxygen vacancy dopes the material by directly providing electrons to the conduction band [62]. Both the 2+ structure and the neutral structure, having an oxygen vacancy but no point defect, are energetically significantly more stable than the structure where a metal—metal bond traps the electrons: we calculate that the formation energy of the metal—metal bond lies between 0.72 and 5.16 eV. This difference indicates that the M-M defects, which were originally formed with the vacancies, have a metastable nature at low electron concentration (i.e., when the Fermi level is in the gap or is reasonably low in the CB).

The formation energies of the combined defects comprising one oxygen vacancy and one metal—metal bond are large: 3.73, 3.38, 2.78, and 1.95 eV. However, once the metal-metal defects are annihilated by a charging-discharging cycle, the formation energy of the oxygen vacancy is substantially lowered to 1.65, 1.61, 1.23, and −1.78 eV in an oxygen-rich environment. The negative value of the last formation energy corresponds to a structure in which a significant atomic reorganization of the amorphous matrix occurs upon the removal of the oxygen. This relaxation is

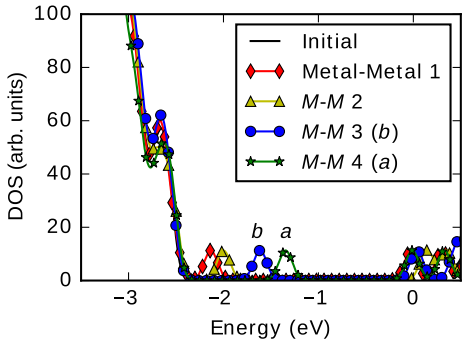

FIG. 2. Densities of states (DOS) of four oxygen deficient models where metal-metal defects are formed. All of the defects form a Kohn-Sham state in the lower part of the gap. The structures and wave functions of the two states labeled a and b are illustrated in Figs. 3(a) and 3(b). The zero of the energy is set to the bottom of the conduction band of the pristine a-IGZO model.

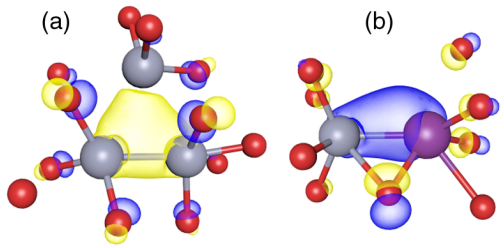

FIG. 3. Illustrations of two "metal—metal bond" defects and their associated isosurfaces of the wave function around the metals involved. (a) Represents the case of a bond formed between two zinc atoms, with a third zinc interacting strongly. (b) Illustrates the bonding of an indium atom with a zinc atom. These illustrations stress that the p orbital of the surrounding oxygen atoms always contributes to the signature of the wave function. This signature clearly distinguishes them from the conduction-band states, as shown in Fig. 11. The contribution of the atoms and of the isosurfaces located far from the central bond are removed for the purpose of illustration. The color of the wave function represents its phase; oxygen atoms are shown in red, indium in purple, and zinc in gray.

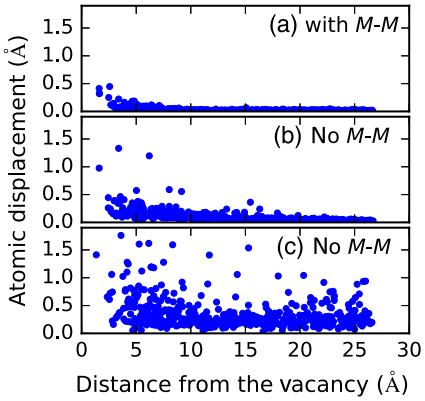

FIG. 4. Atomic displacements induced by the creation of an oxygen vacancy in *a*-IGZO as a function of the distance from the position of the removed oxygen site. In (a), the relaxation is very local and a metal-metal defect is formed. In (b) and (c), the local defect is cured thanks to a large atomic reorganization process.

illustrated in Fig. 4(c) and compared with the reorganization induced by two other vacancies [Figs. 4(a) and 4(b)]. Given the inherent metastability of the amorphous structure, the last oxygen vacancy triggers a relaxation process in an alternative local conformation for the amorphous structure. This reorganization results in a lowering of the global energy by about 0.01 eV/atom with respect to the starting structure, thereby artificially stabilizing the vacancy compared to the initial model. When the formation energy of the vacancy is computed from this newly found local minimum, it rises to 3.5 eV, confirming that the creation of an oxygen vacancy is an endothermic process.

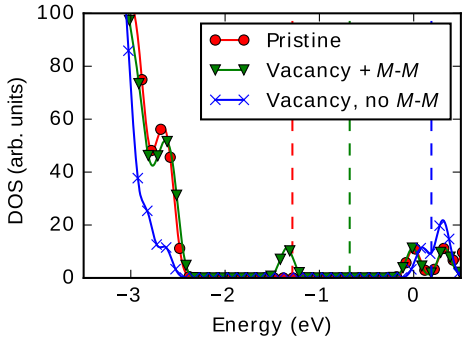

FIG. 5. Densities of states (DOS) for a pristine *a*-IGZO model (the red dots) of a model with an oxygen vacancy and a metal-metal defect (labeled *a* in Fig. 3; the green triangles) and a model with an oxygen vacancy but no metal-metal defect (the blue crosses), obtained by removing and adding back two electrons to the previous model. A state appears in the gap only in the presence of a metal-metal defect. In the last model (the blue crosses), a reorganization of the tail states (states located at the very top of the valence band) occurs, reducing their dispersion. The dashed vertical lines indicate the positions of the Fermi level in the different models. The zero of the energy is set to the bottom of the conduction band of the pristine *a*-IGZO model.

The formation energy of an isolated metal-metal defect can be evaluated by comparing the energies of oxygen-deficient models in the presence and the absence of this point defect. In this situation, the most stable metal-metal defect has a formation energy of 0.72 eV, while the less stable one has a formation energy of 5.16 eV. This energy, however, depends on the position of the Fermi level [57,58], which lies, for the reference structure, in the conduction band due to the presence of a vacancy (see the blue crosses in Fig. 5). Whenever the Fermi level is lowered in the gap, the defect becomes increasingly unstable compared to its ionized counterpart (where no M—M bond exists). In a first approximation, the variation of the formation energy can be estimated by $q\Delta E_f$, where q is the defect charge and ΔE_f the variation of Fermi energy. It hence results that, for a Fermi level positioned at midgap, i.e., at approximately 1.5 eV below the CB, the defect becomes 3 eV less stable than when it is doubly ionized, i.e., upon the breaking of the M—M bond. This change in energy suggests that metal-metal defects become very unstable whenever the Fermi level is set low in the gap. Conversely, the most stable *M*-*M* defect should become stable for a Fermi level located at $0.72/2 = 0.36$ eV above the conduction band. It is nevertheless important to stress that this value needs to be interpreted with caution, as the position of the conduction band is a rather ill-defined concept in an amorphous phase and depends on the model used [61,63]. Also, the formation energies of the *M*-*M* defects largely vary, and some conformations may be more stable than others. Although it is difficult to establish for which value of the Fermi level the metal-metal defects become stable, we expect that a Fermi level lying relatively deep in the conduction bands is required.

For a Fermi level lying in the gap, i.e., at a low electron concentration, the metal-metal defect is metastable, which implies the presence of energetic barriers. The heights of these barriers are expected to be dependent on the Fermi level and are not studied in this work. However, as in the worst-case scenario, the metal—metal bond breaks spontaneously upon ionization, and the barrier must vanish when the Fermi level lies close to the valence-band tail states. For their formation, the conditions for which the barrier vanishes are unclear. We increase the electron concentration in *a*-IGZO to 1.65×10^{21} cm^{-3} by adding ten electrons per unit cell in the pristine model, and we do not observe the formation of any metal—metal bonds upon structural relaxation. Nahm and Kim [35] studied the energetic barrier required for the creation of these metal—metal bonds (more specifically, the In—Ga bond) in a 112-atom model and indicated that the barrier vanishes for a carrier density of about 4.7×10^{21} cm^{-3}, which would require, in our case, the unreasonable addition of 29 electrons. Nahm and Kim also reported that this complex is stable at a carrier concentration of 1.55×10^{21} cm^{-3}, and that, at this point, the height of the formation barrier is 0.49 eV, while the one for

recovery (i.e., to break the bond) is 0.74 eV. By comparison, with the model used in this paper, where the carrier concentration is increased to 3.3×10^{20} cm^{-3} whenever one oxygen vacancy is present, we can crudely estimate that *M*—*M* bonds become thermodynamically stable for a carrier concentration ranging between this concentration of 3.3×10^{20} cm^{-3} (where the defect is metastable) and the one obtained by Nahm and Kim [35] of 1.55×10^{21} cm^{-3}, where it is stable. Finally, the formation barrier at this electron concentration should be larger than the 0.49 eV reported, as the formation energy is expected to increase for lower carrier concentrations. Note that the results of these authors were obtained in the absence of an oxygen vacancy.

In conclusion, the formation of *M*-*M* defects leads to the capture of electrons when the charge concentration is at least 10^{20} cm^{-3}. These defects are easily cured with the lowering of the Fermi level in the gap and remain difficult to form until the Fermi-level position lies deep in the conduction band. We remark that the distinction between *M*-*M* defects and oxygen vacancies was not present in previous studies, as mentioned in the Introduction. *M*-*M* defects have often been described as being neutral oxygen vacancies [17,23,25,33,34] because they easily form whenever an oxygen vacancy is made, thanks to the donor behavior of the vacancy, which raises the electron concentration and enhances the probability of forming a metal-metal defect. This effect is particularly pronounced in small structural models.

B. Peroxide defects

Peroxides result from the covalent bonding of two oxygen atoms. From a simulation perspective, this defect spontaneously forms by adding either one oxygen or two holes in a pristine *a*-IGZO structure. Coherently, with the nomenclature previously defined, both methods are equivalent. Indeed, the addition of an oxygen atom generates a charge imbalance resulting in a +2 charge, equivalent to the injection of two holes in the structure. In practice, upon the injection of holes, the peroxides form by capturing the holes provided. The formation of the peroxide can be understood as the bonding of two oxygen atoms, with each missing an electron. By the formation of a covalent bond between the oxygens, electrons are shared between the two atoms and the missing electrons are no longer needed to satisfy the oxygens. When an oxygen atom is added, it bonds to a metal and to another oxygen to form a peroxide and avoid a positive charging of the system. As discussed later, if the oxygen is added to the system with two electrons, the peroxides do not form because the positive charge due to the cation-anion imbalance is already compensated for by the added electrons.

Both the bonding and antibonding states linked to the peroxide signature lie deep in energy (Fig. 6), with some minor contributions in the upper part of the valence band (Fig. 7, dashed lines). An example of the wave function of this state is illustrated in Fig. 6 (last image, −1.4 eV). It originates from the antibonding interaction between the *p* orbital of the oxygen atoms in the peroxides and is heavily hybridized with the valence-band states (also characterized by antibonding *p* orbitals of various oxygen atoms). The effect of the peroxide on the top of the valence band is hence limited. As shown in Fig. 7, its formation modifies the oxygen contribution in the density of states (DOS), resulting in states that are not significantly different from the original ones or from the rest of the states in the valence band. Since the last occupied states linked to the peroxide lie in the valence bands (or in its tail states), the ionization of the defect is difficult. Indeed, even if ionized, the peroxide is not expected to break since only the antibonding states are depopulated, which actually strengthens the peroxide.

As for the metal-metal defect, the formation energy of a peroxide depends on the position of the Fermi level, and energetic barriers exist to form or cure it. A peroxide forms spontaneously in our model whenever holes are injected. This exoenergetic character indicates the absence of a barrier and a negative formation energy for a Fermi level positioned in, or close to, the valence band. If two electrons

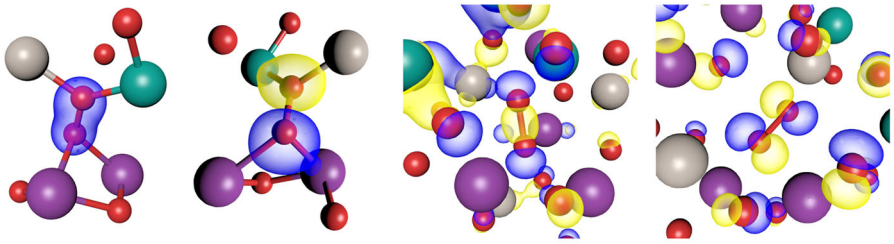

FIG. 6. Illustration of the wave function of the electronic states formed by peroxides in *a*-IGZO. The phases of the electronic wave function are represented in blue and yellow. The energies listed below the states correspond to the energy of the electronic state with respect to the top of the valence band (i.e., the last occupied state of the model). In the two lowest energy states, the electrons are strongly localized on the peroxide and form a simple bonding or antibonding molecular orbital. At high energies, the peroxide contributes to the signature of numerous states, showing a more delocalized signature. These states are divided into two categories: at low energies, the interaction between the atoms of the peroxide is bonding, while at high energies, it is antibonding. The color of the wave function represents its phase. Oxygen atoms are displayed in red, indium in purple, zinc in gray, and gallium in green.

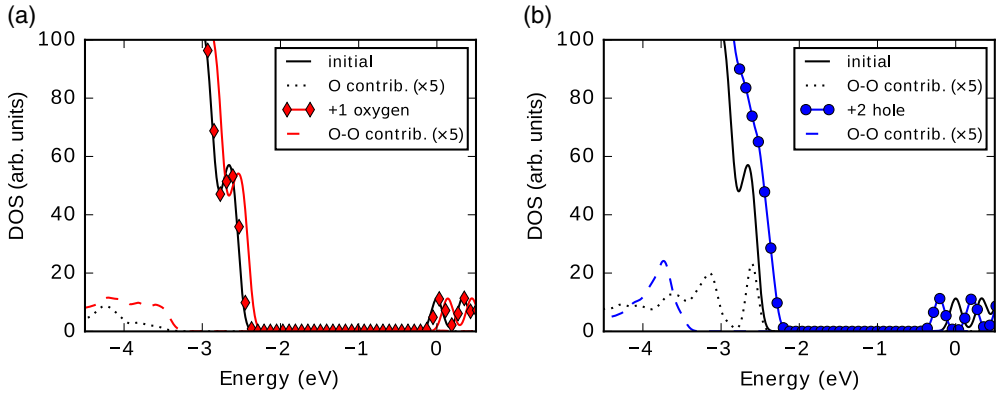

FIG. 7. Densities of states (DOS) of two *a*-IGZO structures owning a peroxide formed (a) by the addition of an oxygen atom (the red diamonds) and (b) by the addition of two holes (the blue dots). The density of states of the initial structure is shown by the continuous black line. The dotted black line in (a) provides the partial DOS of the oxygen atom that is bonded to the added oxygen and, in (b), shows the contribution of the two oxygen atoms contributing to the formation of a peroxide. In the defective structure, the (a) red and (b) blue dashed lines indicate the contribution of the two oxygen atoms forming the peroxide defect. For all structures, E_f is in the band gap. The zero of the energy is set to the bottom of the conduction band of the pristine *a*-IGZO model.

are provided to the system, we observe that the peroxide remains unaltered and that the electrons become delocalized in the conduction band. The stability of the peroxide indicates the presence of a barrier for the recovery process. For a Fermi level lying in the conduction band, enthalpies of formation of 1.58, 1.98, and 1.68 eV are obtained for three different peroxides. The peroxide is hence metastable whenever the Fermi level lies in the conduction band. Our NEB simulations estimate the recovery barrier at 1.1 eV, which indicates that the process is unlikely to occur at room temperature. However, similar to the metal-metal defect, the barrier is expected to decrease when the Fermi-level energy is pushed deeper into the conduction band, meaning that high electron concentrations favor the recovery process of peroxides.

The addition of an oxygen atom in *a*-IGZO does not systematically imply the formation of a peroxide defect. Indeed, as indicated previously, adding one oxygen atom is equivalent to the introduction of two holes to the model, enabling the formation of a peroxide to compensate for these holes. Whenever two electrons are added to the pristine model together with an oxygen atom, an ionic relaxation takes place and the added electrons compensate for the one captured by the oxygen. As a result, no peroxide is formed and the Fermi level remains in the band gap. The additional oxygen simply becomes bonded to a metal site, like any other oxygen atoms in the structure. Because of the formation of this bond, the oxygen atom captures the extra electrons injected, setting the Fermi level in the middle of the gap. This atomic conformation is also 2.98 eV more stable than the alternative one, containing a peroxide with a Fermi level in the conduction band. This difference in energy confirms that whenever the Fermi level is set in the conduction band, the peroxide becomes unstable. However, the peroxide does not break spontaneously: there is an energy barrier for recovery.

The presence of an additional oxygen bonded to a metal generates additional states at the top of the valence band, strongly increasing the valence-band dispersion (and/or tail states), as illustrated in Fig. 8. Note that these higher energy states are indirectly linked to the added oxygen, as reflected by the weak contribution of this oxygen to the valence band in Fig. 8. The origin of these higher energy states is also indistinguishable from other valence-band states. Interestingly, in the opposite case, whenever an oxygen vacancy is formed (Fig. 5), the intensity of the DOS of the valence band tends to decrease. These results suggest that the valence band and its tail states are impacted by the concentration of oxygen, in good agreement with XPS

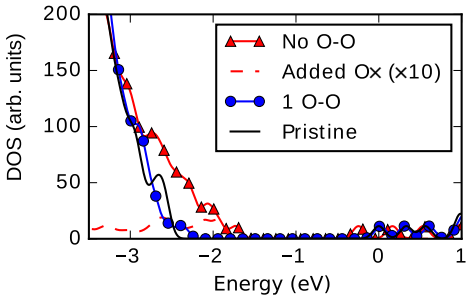

FIG. 8. Densities of states (DOS) of *a*-IGZO in the presence and the absence of a peroxide when one oxygen is added to the model. The continuous black curve indicates the pristine model. The dashed red curve refers to the model without the formation of a peroxide obtained by adding two electrons together with the oxygen atom. The weak contribution of the added oxygen is shown by the red dotted curve. Note that this contribution is magnified 10 times to increase its visibility. The blue dotted curve represents the DOS of the model upon the removal of two electrons and the formation of a peroxide. The zero of the energy is set to the bottom of the conduction band of the pristine *a*-IGZO model.

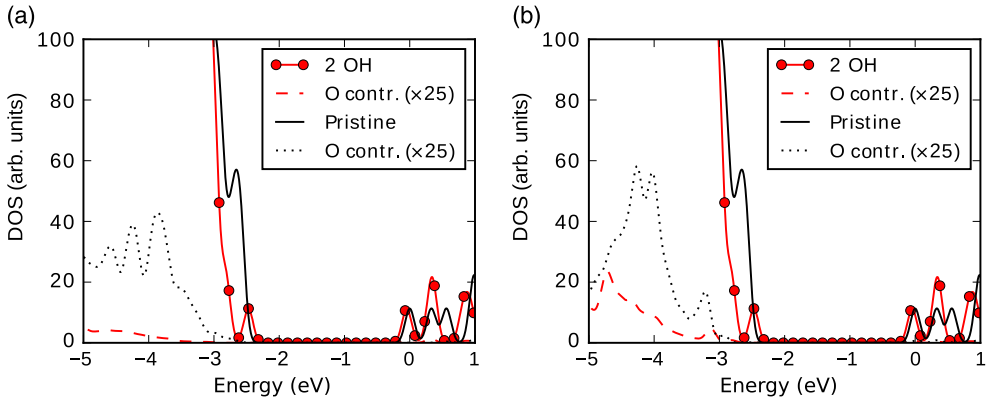

FIG. 9. Density of states (DOS) of an *a*-IGZO model containing two hydroxyl groups (—OH). Figures (a) and (b) provide the contribution of the oxygen before (the dotted black curve) and after (the dashed red curve) binding to a hydrogen atom. The zero of the energy is set to the bottom of the conduction band of the pristine *a*-IGZO model.

results that report an increase in the valence-band tail states with the oxygen concentration [64]. This finding also supports the idea that these tail states mainly originate from the disordered nature of the material and are not specific to point defects.

In conclusion, peroxides are donors that spontaneously form when a sufficient hole density is present in the valence band. Electrons can be recaptured only upon the dissolution of these peroxides, which is a difficult process due to their large recovery barrier. As expected, interstitial oxygens are stoichiometric defects acting as acceptors. They break the balance between metal cations and oxygen anions, resulting in a positive charging of the system.

C. Hydrogen

Hydrogen impurities generate two types of impurities, depending on whether they are bonded to a metal or to an oxygen site. In a pristine *a*-IGZO structure, hydrogen spontaneously bonds to an oxygen atom, forming a hydroxyl group. In the resulting configuration, an electron occupies the conduction band, indicating that the hydrogen acts as a donor. In a hydrogen-rich environment, the computed formation energy of these hydroxyls spans from −0.8 to 0.2 eV, with an average formation energy of −0.4 eV for the six different models built by randomly adding hydrogen atoms to the pristine model. The exoenergetic character of the formation energy indicates that hydroxyl defects tend to spontaneously form in *a*-IGZO. The addition of a hydrogen atom does not generate a state in the gap and tends to push the electronic contribution of the oxygen, on which it is bonded, to a lower energy, as shown in Fig. 9.

The metal-hydrogen (*M*-H) impurity requires the presence of at least one free electron in the model to form. This impurity corresponds, in our case, to a doping of 1.65×10^{20} e/cm^3. After the formation of the defect, the Fermi level returns in the gap, indicating that it captures the provided electron to act as an acceptor. As for most defects in *a*-IGZO, no electronic state is generated in the band gap. Contrary to the hydroxyl (—OH) or the peroxide (O-O) defect, the *M*-H impurity shows some contributions in the DOS at the very top of the valence band, as illustrated in Fig. 10. Although one electron is provided to the extra hydrogen atom, the formed impurity is still metastable and can be broken by forcing the diffusion of the hydrogen toward an oxygen site. This impurity results in the formation of a hydroxyl defect which is, in this situation, approximately 0.7 eV more stable. The presence of a large activation energy (1.63 eV) nonetheless indicates that this diffusion is particularly difficult. Interestingly, if an electron is further removed from the model (i.e., if the electron concentration is decreased), the barrier for the diffusion of the hydrogen decreases but remains significant (0.73 eV). This barrier suggests that, once the *M*-H defect is formed, it is particularly difficult to break. Note that the *M*-H defect becomes highly metastable in the case of an injection of an extra electron, as the O-H defect becomes more stable by 2.53 eV (instead of 0.7 eV).

The results suggest that hydrogen tends to bind itself to oxygen and to act as a donor until a high electron concentration is achieved ($>1.65 \times 10^{20}$ e/cm^3). At this point, hydrogen starts to bind to metal sites, forming acceptors which compensate for the surplus of electrons in the material. *M*-H defects could also form during the deposition and, although they are unstable for a Fermi level

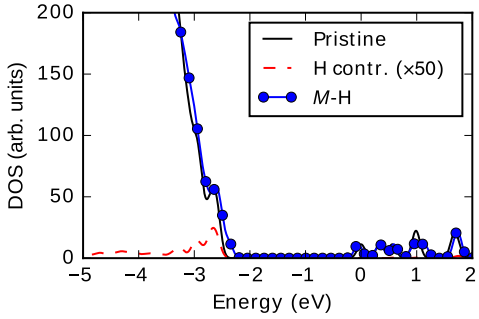

FIG. 10. Density of states (DOS) of a model containing a metal-hydrogen impurity with an additional electron (the blue circles). The pristine DOS is provided by the continuous black line, and the contribution of hydrogen, at the very top of the valence band, is shown by the dashed red line. The zero of the energy is set to the bottom of the conduction band of the pristine *a*-IGZO model.

TABLE II. Summary of the formation energies and barriers discussed in this work. The defect formation energies are dependent on the Fermi level. Hydrogen impurities and oxygen vacancies or interstitials also depend on the chemical potential of the oxygen or hydrogen species. In this table, oxygen- and hydrogen-rich conditions are assumed. Unless stated otherwise, the formation energies are computed using the neutral pristine model as reference. The formation energies obtained with a charged pristine model as reference are annotated with square brackets, indicating the charge of the unit cell. The number in parentheses indicates the number of defects considered. For the barriers, the square brackets provide the carrier concentration in the initial model (the carrier concentration change following the creation or dissolution of the defect). In our model, $1e^-$ in the conduction band (CB) is equivalent to an electron concentration of 1.65×10^{20} cm^{-3}.

Defect	Type	Formation energy	Barrier
M-*M*	Acceptor	0.72–5.16 eV (4)	Creation: 0.49 eV [$c = 1.55 \times 10^{21}$ cm^{-3}] (1) [35]
O-O	Donor	1.6 eV (1) 2.98 eV (1) [$2e^-$ in CB]	Dissolution: 1.1 eV [$2e^-$ in CB] (1)
O interstitial	Acceptor	−1.14 eV (1) [$2e^-$ in CB]	
O vacancy	Donor	1.23–1.65 eV (3)	
M-H	Acceptor	0.6 eV (1) [$1e^-$ in CB]	*M*-H => O-H: 1.63 eV (1)
O-H	Donor	(−0.8)–0.2 eV (6)	

lying in the gap, they may still be present due to their large barrier for recovery. Metal-hydrogen impurities are, hence, rather difficult to form or to break. In the presence of hydrogen, this mechanism should therefore limit the maximum doping concentration achievable in *a*-IGZO. We remind the reader that metal—metal bonds are also able to capture electrons in these conditions. Therefore, it is *a priori* uncertain whether metal-metal or *M*-H defects will ultimately set the doping limits.

D. Summary

Table II summarizes the formation energies and barriers of creation or dissolution of the different defects discussed. All defects have barriers for their creation or dissolution. For hydrogen, oxygen vacancies, and interstitials, they are set by the diffusion barriers of oxygen and hydrogen, which are not investigated. For *M*-*M* defects and peroxides, the barriers depend on the Fermi level and always cancel out at some point. For *M*-*M* defects, creation is spontaneous at high electron concentration, while the formation of peroxide is spontaneous at low hole concentration. The presence of barriers indicates that all of the defects may be metastable, resulting in instabilities, as discussed in the following section.

IV. DOPING MECHANISM IN *a*-IGZO

Oxygen vacancies are often considered to be at the origin of the intrinsic electron doping in *a*-IGZO transistors. The major argument is that oxygen annealing reduces the carrier concentration [6,46,65,66]. Nomura *et al.* [67], however, showed that *a*-IGZO films unintentionally contain large amounts of hydrogen ($>10^{20}$ cm^{-3}), but they still show carrier concentrations as low as 10^{15} cm^{-3}. As both oxygen vacancies and hydrogen act as donors, the low carrier concentration cannot be explained by the presence of oxygen vacancies alone since they should, according to our findings, further increase the doping concentration. An excess of oxygen, as suggested by Nomura *et al.* [67], could compensate for the surplus of hydrogen. This vision is confirmed by our calculations. First, hydrogen defects (–OH) have a negative formation energy, implying a spontaneous formation of these defects whenever hydrogen is present. Since oxygen vacancies have larger formation energies (up to 2 eV higher), our results point to the contribution of hydrogen as being the dominant source of doping in *a*-IGZO. Second, it is shown that extra oxygen atoms act as electron acceptors. It hence results that, in the presence of hydrogen, the reduction of the carrier concentration upon oxygen annealing can be explained by the inclusion of an excess of oxygen bonding to the metals, compensating for the hydrogen donor contribution. Some compensation mechanism may also arise from the formation of *M*-H defects created during the deposition and are preserved thanks to their large barrier for recovery. While the compensation originating for additional oxygen atoms should be stable, the one based on *M*-H defects should decrease with time and lead to an increase of the electron doping of the material upon aging.

Following our theoretical results, neither the presence of –OH defects nor the oxygen in excess is expected to have a large impact on the transistor characteristics of *a*-IGZO. These two types of defects impact only the valence-band tail states, and they do so in opposite ways: hydrogen tends to push the energy states of oxygen to a lower energy, reducing the tail states, while the addition of oxygen atoms increases the number of states in the valence band and hence the probability of forming tail states. The excess of oxygen and hydrogen in the layers can, however, deteriorate the stability of these TFTs, as discussed in the next section.

None of the defects studied generate an electronic state close to the conduction band. Contrary to the valence band, additional tail states are not directly observed in the density

of states of the pristine model. This absence raises the question of the nature of the tail states reported experimentally [1] close to the conduction band. Although the model studied in this work is relatively large, the absence of tail states can still be explained by its restricted dimensions. Indeed, the comparison of the electronic structures of the various models used for the creation of defects reveals that the first conduction-band state adopts a wide distribution in energy, depending on its degree of delocalization, as illustrated in Fig. 11. The mechanisms that dictate this localization (or delocalization) in our different models

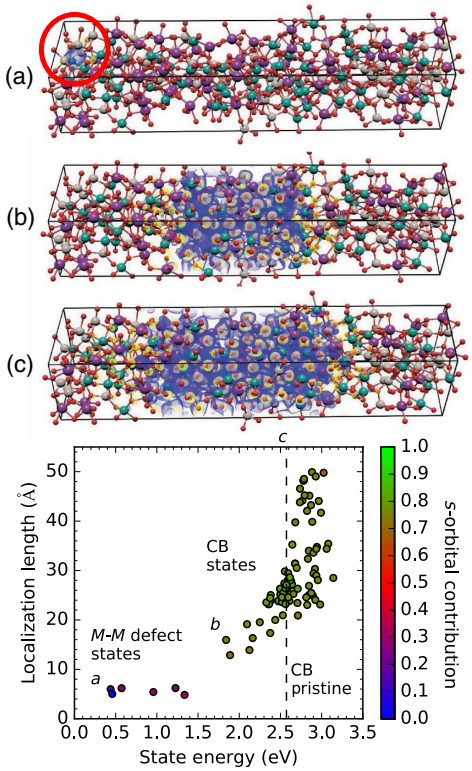

FIG. 11. Delocalization length of electronic states where metals interact in the band gap for various models with and without defects. The color scale in the graph indicates the contribution of the *s* orbital in the state. The zero of the energy is set at the last tail states of the pristine *a*-IGZO model. The delocalization width is obtained by a Gaussian fitting of the wave function after its projection in the elongated direction of the model. Note that the method is not accurate when the delocalization length comes close to the dimension of the model (i.e., approximately 5 nm) or for harmonics of the first conduction band (see Ref. [38] for details). The zero of the energy is set at the highest-energy valence-band state (a tail state) of the pristine model. The position of the conduction band of this pristine model is depicted by the dashed lines. The states in the gap at the lowest energy are due to metal—metal bond defects. Representations of the wave functions of three states labeled *a*, *b*, and *c* are provided at the top of the figure. (a) The lowest-energy metal-metal state, where the red circle indicates the position of the defect. (b) The lowest-energy conduction-band state. (c) The first conduction band of the pristine model.

remain, however, unclear. In particular, we observe that no specific correlations exist with respect to the presence and/or the position of the defects. Nonetheless, the variation of the energy of the first conduction-band state can explain the tail states observed experimentally and suggests that they would correspond to the signature of the most-localized conduction-band states. They are, however, not captured in the models used in this work due to their dimensions. Ideally, capturing this distribution would require modeling systems of at least 1 order of magnitude larger than the size of the localization of the conduction-band states, which is already on the order of a few nanometers.

The position of the Kohn-Sham states and the localization length of metal-metal defects are also provided in Fig. 11. In a first-order approximation, one can consider these defects extreme cases of the conduction-band localization, where only a very few metal sites interact (leading to strongly localized states). Nonetheless, these states are characterized by a much lower contribution of the *s* orbital which dominates the conduction-band states, as shown in Fig. 11. Note that the most-localized conduction-band states also tend to have lower *s*-orbital contributions, to the benefit of directional *p* orbitals.

V. INSTABILITIES MECHANISM IN *a*-IGZO

The overview of the defective models developed in the previous paragraphs hints at potential mechanisms for instabilities in *a*-IGZO transistors. In the following, the three major instabilities encountered in *a*-IGZO TFTs, namely, the NBS, the PBS, and the NBIS, are discussed. The discussion focuses on the identification of the mechanisms linked to the presence of defects in the *a*-IGZO channel. It must be underscored that charge trapping at interfaces and in the dielectric of a transistor probably also contribute to these instabilities but are not considered in this discussion. Numerous sources suggest that the creation of defects could not be at the origin of NBS and/or PBS instabilities because the subthreshold slope is not significantly modified in the process [7,9]. This conclusion finds its root in the erroneous idea that the creation of a defect systematically induces an electronic state in the band gap and hence leads to an increase of the subthreshold slope of the transistor. While this is a relevant picture for classical CMOS transistors using crystalline materials for their channel, the discussion above shows that this picture is inaccurate in the case of *a*-IGZO. Indeed, our theoretical findings suggest that many defects do form without inducing a defect state in the electronic band gap. They can, therefore, give rise to threshold-voltage instabilities that are not accompanied by degradation of the subthreshold slope.

A. Negative-bias stress

Negative-bias stress instabilities refer to the negative shift of the transfer curve (drain-source current vs gate

voltage) of TFTs upon the application of a prolonged negative gate bias. The occurrence of the shift is slow (hours) and time dependent. It preserves the transistor mobility and its subthreshold slope, and the device recovers once the stress is removed [6,7]. It also increases with the amplitude of the applied gate bias and with temperature [23]. NBS instability is improved in the presence of high-quality interfaces and when a good passivation layer is set in contact with the dielectrics [6,30].

A possible explanation for the origin of the NBS is the creation of donors in *a*-IGZO. Indeed, upon the application of a negative gate-bias stress, the Fermi level is pushed towards the valence band, which results in a decrease of the formation energy of donors. If the bias stress is maintained, the lowered formation energy leads to a new thermodynamic equilibrium state, with a large steady-state concentration of donor defects. When the kinetics of the reaction is sufficiently fast, the stress causes an increase of the donor concentration in the channel, shifting the transfer curve, as has been observed experimentally [6,7]. Set in perspective with our results, three types of defects could be responsible for this effect: the creation of oxygen vacancies [23] or of peroxides or the diffusion of hydrogen (O-H formation). The creation of peroxides can be dismissed as the primary source of contribution since, according to the simulations, peroxides are associated with high-recovery energy barriers. Should peroxide formation be the root cause of NBS, the threshold voltage shift would essentially not be recoverable with time, while, experimentally, recovery is reported to be of the same order as the stressing time [23]. Nevertheless, a minor contribution of peroxides may not be excluded and would be responsible for a partial lack of recovery. Considering the other two options, the formation of oxygen vacancies or of O—H bonds, they require, respectively, out-diffusion of oxygen or in-diffusion of hydrogen. From a kinetic point of view, both species have a high diffusivity in *a*-IGZO [67,68], indicating that a diffusion-based mechanism is possible to explain the kinetics of NBS. For oxygen, this process is further supported by the fact that resistive memories are reported based on *a*-IGZO and their switching mechanism is based on the in- and out-diffusion of oxygen [69,70]. From an energetic point of view, the interaction of the hydrogen with oxygen has a lower enthalpy of formation (about −0.4 eV in a hydrogen-rich environment, mean value) than the formation of oxygen vacancies (about 1.5 eV in oxygen-rich environment, mean value). However, while the presence of hydrogen dopes the system with a single electron per impurity, oxygen vacancies dope it with two electrons per defect. As the formation energy of the defect decreases with the number of charges it injects, the formation energy of the oxygen vacancy decreases twice as fast with the electron concentration as with hydrogen. This reduction results in a stronger thermodynamic drive for the creation of oxygen vacancies than for the creation of O-H impurities.

The diffusion of oxygen and/or hydrogen is also compatible with experiential observations about NBS [6,6,7,30]: the shift is slow and progressive as the oxygen (hydrogen) needs time to defuse out of (in) the channel. The recovery should occur in a similar timescale as the diffusion because this process is reversible if we assume that the oxygen (hydrogen) is not trapped at the interface, in the dielectric, or at the contacts. As discussed previously, the mobility and the subthreshold slope should not be impacted, as neither hydrogen nor oxygen defects form states close to the conduction band. The increase in NBS with the gate voltage is explained by the fact that, under larger negative bias, the Fermi level shifts deeper in the band gap, closer to the valence-band edge, which decreases the formation energy of the vacancies (–OH defects) and hence increases the thermodynamic drive for the diffusion and, finally, promotes the NBS shift. Last, the temperature dependence may simply be explained by the increase of oxygen and/or hydrogen diffusion, which drives the speed at which the transfer curve shifts.

An alternative explanation for NBS may involve the disappearance of acceptor defects created during the deposition process instead of the creation of donor defects. In this scenario, the breaking of metal-metal defects [17,25] and the diffusion of hydrogen atoms from metal to oxygen should be considered. The breaking of metal-metal defects is expected to be an easy process, and they are not expected to reform unless the Fermi level is raised deep in the conduction band. This instability leads us to conclude that metal-metal defects are poor candidates for NBS. The breaking of a *M*-H defect is also unlikely to occur for similar reasons: O-H defects are more stable than *M*-H defects, even when the Fermi level is located at the bottom of the conduction band. This breaking would make the recovery process unlikely, in contradiction to experimental reports [6,7,23]. Nonetheless, minor contributions of these defects cannot be excluded and may result in a partial nonrecovery of NBS.

B. Positive-bias stress

Positive-bias stress instability refers to the shift of the transistor curve during prolonged application of a positive gate bias. The TFT mobility and subthreshold slope are not affected in PBS [6,7]. The device recovers from the instability and the process is measured to be temperature dependent [9,14].

PBS can be explained by the removal of hydrogen and/or by the filling of the oxygen vacancies, using the same arguments as were expressed for NBS. A positive gate bias pushes the Fermi level towards (into) the conduction band and increases the formation energies of both the oxygen vacancies and the –OH defects. This increase provides a thermodynamic drive to reduce the defect concentration, lessening the doping of the layer and shifting the transistor threshold voltage positively. This model for PBS is supported by recent technology computer-aided design (TCAD) simulations [19], showing a good fit of experimental transfer

curves shift under PBS by considering a hydrogen diffusion process out of the channel layer.

Note, however, that the change in the position of the Fermi level in PBS is expected to be smaller than the one in NBS. Indeed, the position of the Fermi level in a TFT is driven by the variation of charges at the gate. Given that the Fermi level is expected to be close to the conduction band because *a*-IGZO is naturally *N* doped, a negative bias could *easily* decrease the Fermi level deep into the gap (which is about 3 eV wide). In PBS, however, the same gate voltage may induce a smaller shift of the Fermi level since, once it reaches the bottom of the conduction band, the increase of the gate voltage is limited by the large conduction-band density of states.

Interestingly, devices with large PBS tend to have small NBS, while devices with small PBS tend to show high NBS [6,7,71]. Assuming that both NBS and PBS are driven by diffusion processes, the variation of NBS versus PBS can be linked to the ability of the surrounding material to accept or not accept hydrogen and/or oxygen. For instance, if an interface material is oxygen rich, oxygen is more likely to diffuse into the channel than out of it, leading to a stronger PBS than NBS. However, both instabilities should be reduced by designing interfaces blocking the diffusion of oxygen and hydrogen in the channel layer. Obviously, a low concentration of hydrogen should also be beneficial.

Another plausible explanation for the occurrence of PBS is the reduction of naturally present peroxide defects in the IGZO film. Indeed, thanks to their large barrier for recovery, peroxides created during the deposition may be preserved for very long time spans. Upon application of an elongated positive bias, their dissolution barrier decreases, increasing the probability of breaking these peroxides. This process should nonetheless be irreversible, as peroxides are not expected to reform easily unless the electron concentration in the film becomes very low.

PBS could, alternatively, be explained by the formation of metal—hydrogen bonds or of metal-metal defects, which are both acceptor sources able to shift the threshold voltage positively. Our simulations indicate that these defects are difficult to form due to their large enthalpy of formation and to the presence of an energetic barrier for their formation. Although unlikely, this formation could nonetheless still be consistent with the long bias time needed to obtain a significant shift of the transfer curve. Speaking against *M*-H or *M*-*M* defects as sources of PBS is the fact that it is expected that, in most cases, the Fermi level may not be positioned high enough in the conduction band for these defects to be stable. Also, the experimentally observed recovery process is not in accordance with what would be expected for *M*-*M* defects (which dissolve quickly) and *M*-H defects (the dissolution of which is difficult).

C. Negative-bias illumination stress

Negative-bias illumination stress combines a prolonged negative-bias stress and excitation by light. Similar to NBS, it results in a negative shift of the threshold voltage. However, the shift observed is always substantial (even if the effect of NBS is negligible), provided that the photon energy used for the illumination process is important enough [30]. Unlike NBS, NBIS does not recover easily [10,11]. Depending on the quality of the layer and of the interfaces, the photon energy required to induce NBIS can range from 2.3 eV (where deep tail states are probed) to above 3 eV (where valence-band states are excited) [30].

NBIS has been explained by the creation of a peroxide defect [5,15,31,36,37], which easily forms when the Fermi level is close to or into the valence band. Peroxides form by the capture of two holes, i.e., by the bonding of two oxygen atoms missing an electron. A large density of holes is required in order to have two neighboring oxygen atoms missing an electron and triggering the formation of the defect. But the diffusion of holes is difficult because they are easily tapped into polarons, which diffuse poorly [37]. Therefore, holes cannot simply be injected from the contacts, and thus the density of holes in the film remains negligible under negative gate-bias stress alone. With the addition of light excitation, electrons of the tail states of the valence band are excited to the conduction band and are evacuated by the source-drain contacts because of the simultaneous application of a negative gate bias. Thus, a large number of holes are created in the valence-band states, and they can interact to form peroxides, as peroxides are metastable complexes. The slow and incomplete recovery of NBIS can be explained by the fact that formed peroxides do not dissolve, even when the bias is removed and the Fermi level is pushed back into the band gap—or even into the conduction band.

This picture is compatible with the explanation of NBS, in the sense that NBIS can inhibit NBS. Indeed, because the peroxide captures two holes, it globally charges the material $+2|e^-|$, which counteracts the negative gate bias, reducing the effective bias of the channel. Consequently, this process reduces the thermodynamic drive for the creation of vacancies or -OH defects and lessens the NBS shift in favor of a more permanent NBIS shift.

As another potential mechanism for NBIS, we dismiss the options of the creation of vacancies and of a hydrogen diffusion process because they should be readily recoverable. Mechanisms involving the breaking of either metal-metal defects or *M*—H bonds (to create O—H bonds) offer an alternative explanation. Indeed, these two defects contribute to the electronic signature of the top of the valence band, and even to gap states (for *M*-*M* complex), which could then be excited by light illumination, resulting in a breaking of the *M*—*H* or *M*—*M* bonds. However, given that *M*—*M* bonds are easy to break and are quite unstable, they are also unlikely candidates to dominate the NBIS process. The case of *M*-H defects is more complex. Indeed, while they are unstable, a large barrier for recovery is observed, implying that whenever a *M*-H defect is formed during the material growth, it can participate in the NBIS

instability process, a was recently suggested by Bang *et al.* [72]. In this situation, NBIS should, however, not recover at all because the *M*-H defects were originally metastable. Hence, once the *M*—H bond breaks, they should not reform, even after annealing.

VI. CONCLUSIONS

In this paper, a rational classification of the behavior of defects in *a*-IGZO is proposed on the basis of a distinction between point defects and nonstoichiometric defects. Point defects are strictly characterized by local deformations of the amorphous matrix. Their stability is dependent on the position of the Fermi level in the material, and some energetic barriers exist to create or cure them. Nonstoichiometric defects are always shallow and are obtained by modifying the stoichiometry of the material. They can be created or removed only by diffusion.

Two types of intrinsic point defects are discerned: metal-metal defects, acting as an acceptor source that captures two electrons, and the O-O (peroxide) defects, which act as a donor able to provide two electrons to the system. A metal-metal complex is stable under a large electron concentration and becomes metastable to finally spontaneously break whenever the Fermi level is moved low in the band gap. By contrast, peroxides are stable for a Fermi level in or close to the valence band and are metastable whenever it rises into the conduction band.

Nonstoichiometric defects are characterized by more-subtle atomic rearrangements, able to dope the material without requiring the creation of a point defect. The resulting doping is perfect and is independent of the position of the Fermi level. Two main types of stoichiometric defects are distinguished in *a*-IGZO: oxygen vacancies obtained by the removal of oxygen, acting as donors, and oxygen interstitial defects generated by the addition of oxygen, acting as acceptors. Stoichiometric defects can be created by the diffusion of species into or out of the material. In this regard, a variation of the position of the Fermi level can impact the diffusion by modulating the formation energies of these defects.

Impurities and intrinsic point defects share similar characteristics. Hydrogen in *a*-IGZO forms two types of impurities. Once formed, the metal-hydrogen defect acts as a single electron acceptor, and it is only stable for a Fermi level positioned high in the conduction band. It becomes metastable whenever the Fermi level is moved into the band gap. For low electron doping, the formation of oxygen-hydrogen defects is preferred and acts as a single electron donor source.

ACKNOWLEDGMENTS

We acknowledge the use of the PYMATGEN [73] and PYCP2K libraries for data processing. 3D plots are rendered with BLENDER using the ATOMIC BLENDER add-on and JMOL.

[1] Toshio Kamiya and Hideo Hosono, Material characteristics and applications of transparent amorphous oxide semiconductors, NPG Asia Mater. **2**, 15 (2010).

[2] Yoshiharu Kataoka, Hajime Imai, Yukinobu Nakata, Tohru Daitoh, Takuya Matsuo Naofumi Kimura, Taketoshi Nakano, Yukio Mizuno, Taimi Oketani, Masahiro Takahashi, Masashi Tsubuku, Hiroyuki Miyake, Tetsuji Ishitani Yoshiharu Hirakata, Jun Koyama, Shunpei Yamazaki, Junichi Koezuka, and Kenichi Okazaki, 56.1: Development of IGZO-TFT and creation of new devices using IGZO-TFT, SID Symp. Dig. Tech. Pap. **44**, 771 (2013).

[3] Toshiaki Arai and Tatsuya Sasaoka, 49.1: Invited paper: Emergent oxide TFT technologies for next-generation AM-OLED displays, SID Symp. Dig. Tech. Pap. **42**, 710 (2011).

[4] Jang Yeon Kwon and Jae Kyeong Jeong, Recent progress in high performance and reliable *n*-type transition metal oxide-based thin film transistors, Semicond. Sci. Technol. **30**, 024002 (2015).

[5] Jae Kyeong Jeong, Photo-bias instability of metal oxide thin film transistors for advanced active matrix displays, J. Mater. Res. **28**, 2071 (2013).

[6] Wei Tsung Chen, Shih Yi Lo, Shih Chin Kao, Hsiao Wen Zan, Chuang Chuang Tsai, Jian Hong Lin, Chun Hsiang Fang, and Chung Chun Lee, Oxygen-dependent instability and annealing/passivation effects in amorphous In-Ga-Zn-O thin-film transistors, IEEE Electron Device Lett. **32**, 1552 (2011).

[7] A. Suresh and J. F. Muth, Bias stress stability of indium gallium zinc oxide channel based transparent thin film transistors, Appl. Phys. Lett. **92**, 033502 (2008).

[8] Ajay Bhoolokam, Characterization of amorphous indium gallium zinc oxide thin film transistors, Ph.D. thesis, Katholieke Universiteit Leuven, 2016.

[9] Hui-Min Qian, Guang Yu, Hai Lu, Chen-Fei Wu, Lan-Feng Tang, Dong Zhou, Fang-Fang Ren, Rong Zhang, You-Liao Zheng, and Xiao-Ming Huang, Temperature-dependent bias-stress-induced electrical instability of amorphous indium-gallium-zinc-oxide thin-film transistors, Chin. Phys. B **24**, 077307 (2015).

[10] Sungsik Lee, Arokia Nathan, Sanghun Jeon, and John Robertson, Oxygen defect-induced metastability in oxide semiconductors probed by gate pulse spectroscopy, Sci. Rep. **5**, 14902 (2015).

[11] Md Delwar Hossain Chowdhury, Piero Migliorato, and Jin Jang, Temperature dependence of negative bias under illumination stress and recovery in amorphous indium gallium zinc oxide thin film transistors, Appl. Phys. Lett. **102** (2013).

[12] Jae Kyeong Jeong, The status and perspectives of metal oxide thin-film transistors for active matrix flexible displays, Semicond. Sci. Technol. **26**, 034008 (2011).

[13] Jae Kyeong Jeong, Photo-bias instability of metal oxide thin film transistors for advanced active matrix displays, J. Mater. Res. **28**, 2071 (2013).

[14] Md Delwar Hossain Chowdhury, Piero Migliorato, and Jin Jang, Time-temperature dependence of positive gate bias stress and recovery in amorphous indium-gallium-zinc-oxide thin-film-transistors, Appl. Phys. Lett. **98**, 153511 (2011).

[15] W. H. Han, Y. J. Oh, K. J. Chang, and Ji-Sang Park, Electronic Structure of Oxygen Interstitial Defects in Amorphous In-Ga-Zn-O Semiconductors and Implications for Device Behavior, Phys. Rev. Applied **3**, 044008 (2015).

[16] W. H. Han and K. J. Chang, Subgap States Near the Conduction-Band Edge due to Undercoordinated Cations in Amorphous In-Ga-Zn-O and Zn-Sn-O Semiconductors, Phys. Rev. Applied **6**, 044011 (2016).

[17] Hyeon-Kyun Noh, K. J. Chang, Byungki Ryu, and Woo-Jin Lee, Electronic structure of oxygen-vacancy defects in amorphous In-Ga-Zn-O semiconductors, Phys. Rev. B **84**, 115205 (2011).

[18] S. Choi, J. Jang, H. Kang, J. H. Baeck, J. U. Bae, K. S. Park, S. Y. Yoon, I. B. Kang, D. M. Kim, S. J. Choi, Y. S. Kim, S. Oh, and D. H. Kim, Systematic decomposition of the positive bias stress instability in self-aligned coplanar In-Ga-Zn-O thin-film transistors, IEEE Electron Device Lett. **38**, 580 (2017).

[19] Sungwon Kong, Stephen Wilson, Derek Kimpton, and Eric Guichard, P-4: TCAD simulation of hydrogen diffusion induced bias temperature instability in *a*-IGZO thin-film transistors, SID Symp. Dig. Tech. Pap. **48**, 1238 (2017).

[20] Kay Domen, Takaya Miyase, Katsumi Abe, Hideo Hosono, and Toshio Kamiya, Positive-bias stress test on amorphous In-Ga-Zn-O thin film transistor: Annealing-temperature dependence, J. Disp. Technol. **10**, 975 (2014).

[21] Kwang Hwan Ji, Ji In Kim, Hong Yoon Jung, Se Yeob Park, Rino Choi, Un Ki Kim, Cheol Seong Hwang, Daeseok Lee, Hyungsang Hwang, and Jae Kyeong Jeong, Effect of high-pressure oxygen annealing on negative bias illumination stress-induced instability of InGaZnO thin film transistors, Appl. Phys. Lett. **98**, 3 (2011).

[22] Himchan Oh, Sung Min Yoon, Min Ki Ryu, Chi Sun Hwang, Shinhyuk Yang, and Sang Hee Ko Park, Photon-accelerated negative bias instability involving subgap states creation in amorphous In-Ga-Zn-O thin film transistor, Appl. Phys. Lett. **97**, 1 (2010).

[23] Albert de Jamblinne de Meux, Ajay Bhoolokam, Geoffrey Pourtois, Jan Genoe, and Paul Heremans, Oxygen vacancies effects in *a*-IGZO: Formation mechanisms, hysteresis, and negative bias stress effects, Phys. Status Solidi (a) **214**, 1770131 (2017).

[24] Bo-Wei Chen, Ting-Chang Chang, Shin-Ping Huang, Chih-Hung Pan, and Yu-Ju Hung, Abnormal transconductance enhancement effects induced by negative bias-stress at high temperature in amorphous-In-Ga-Zn-O thin-film transistors, in *Proceedings of the 2016 IEEE 16th International Conference on Nanotechnology (IEEE-NANO), Sendai, Japan, 2016* (IEEE, New York, 2016), p. 780.

[25] Byungki Ryu, Hyeon-Kyun Noh, Eun-Ae Choi, and K. J. Chang, O-vacancy as the origin of negative bias illumination stress instability in amorphous In-Ga-Zn-O thin film transistors, Appl. Phys. Lett. **97**, 022108 (2010).

[26] Young Jun Oh, Hyeon-Kyun Noh, and Kee Joo Chang, The effects of electric field and gate bias pulse on the migration and stability of ionized oxygen vacancies in amorphous In-Ga-Zn-O thin film transistors, Sci. Technol. Adv. Mater. **16**, 034902 (2015).

[27] Jozeph Park, Chang-Sun Kim, Byung Du Ahn, Hojun Ryu, and Hyun-Suk Kim, Flexible In-Ga-Zn-O thin-film transistors fabricated on polyimide substrates and mechanically induced instability under negative bias illumination stress, J. Electroceram. **35**, 106 (2015).

[28] M. P. Hung, D. Wang, J. Jiang, and M. Furuta, Negative bias and illumination stress induced electron trapping at back-channel interface of InGaZnO thin-film transistor, ECS Solid State Lett. **3**, Q13 (2014).

[29] Hyo Jin Kim Jeong, Se Yeob Park, Hong Yoon Jung, Byeong Geun Son, Chang-Kyu Lee, Chul-Kyu Lee, Jong Han Jeong, Yeon-Gon Mo, Kyoung Seok Son, Myung Kwan Ryu, Sangyoon Lee, and Jae Kyeong, Role of incorporated hydrogen on performance and photo-bias instability of indium gallium zinc oxide thin film transistors, J. Phys. D **46**, 055104 (2013).

[30] Kenji Nomura, Toshio Kamiya, and Hideo Hosono, Highly stable amorphous In-Ga-Zn-O thin-film transistors produced by eliminating deep subgap defects, Appl. Phys. Lett. **99**, 053505 (2011).

[31] Ho-Hyun Nahm, Yong-Sung Kim, and Dae Hwan Kim, Instability of amorphous oxide semiconductors via carrier-mediated structural transition between disorder and peroxide state, Phys. Status Solidi (b) **249**, 1277 (2012).

[32] Youngho Kang, Byung Du Ahn, Ji Hun Song, Yeon Gon Mo, Ho-Hyun Nahm, Seungwu Han, and Jae Kyeong Jeong, Hydrogen bistability as the origin of photo-bias-thermal instabilities in amorphous oxide semiconductors, Adv. Electron. Mater. **1**, 1400006 (2015).

[33] Wolfgang Korner, Daniel F. Urban, and Christian Elsasser, Origin of subgap states in amorphous In-Ga-Zn-O, J. Appl. Phys. **114**, 163704 (2013).

[34] Toshio Kamiya, Kenji Nomura, and Hideo Hosono, Subgap states, doping and defect formation energies in amorphous oxide semiconductor *a*-$InGaZnO_4$ studied by density functional theory, Phys. Status Solidi (a) **207**, 1698 (2010).

[35] Ho-hyun Nahm and Yong-sung Kim, Under-coordinated indium as an intrinsic electron trap center in amorphous $InGaZnO_4$, NPG Asia Mater. **6**, e143 (2014).

[36] John Robertson and Yuzheng Guo, Light induced instability mechanism in amorphous InGaZn oxide semiconductors, Appl. Phys. Lett. **104**, 162102 (2014).

[37] A. de Jamblinne de Meux, G. Pourtois, J. Genoe, and P. Heremans, Effects of hole self-trapping by polarons on transport and negative bias illumination stress in amorphous-IGZO, J. Appl. Phys. **123**, 161513 (2018).

[38] Albert de Jamblinne de Meux, Geoffrey Pourtois, Jan Genoe, and Paul Heremans, Origin of the apparent delocalization of the conduction band in high mobility amorphous semiconductors, J. Phys. Condens. Matter **29**, 255702 (2017).

[39] John P. Perdew, Adrienn Ruzsinszky, Gábor I. Csonka, Oleg A. Vydrov, Gustavo E. Scuseria, Viktor N. Staroverov, and Jianmin Tao, Exchange and correlation in open systems of fluctuating electron number, Phys. Rev. A **76**, 040501 (2007).

[40] Fumiyasu Oba, Atsushi Togo, Isao Tanaka, Joachim Paier, and Georg Kresse, Defect energetics in ZnO: A hybrid Hartree-Fock density functional study, Phys. Rev. B **77**, 245202 (2008).

[41] M. Marsman, J. Paier, A. Stroppa, and G. Kresse, Hybrid functionals applied to extended systems, J. Phys. Condens. Matter **20**, 064201 (2008).

[42] John P. Perdew, Kieron Burke, and Matthias Ernzerhof, Generalized Gradient Approximation Made Simple, Phys. Rev. Lett. **77**, 3865 (1996).

[43] Manuel Guidon, Jürg Hutter, and Joost VandeVondele, Robust periodic Hartree-Fock exchange for large-scale simulations using Gaussian basis sets, J. Chem. Theory Comput. **5**, 3010 (2009).

[44] Manuel Guidon, Jürg Hutter, and Joost VandeVondele, Auxiliary density matrix methods for Hartree-Fock exchange calculations, J. Chem. Theory Comput. **6**, 2348 (2010).

[45] T. Kamiya, K. Nomura, and H. Hosono, Origins of high mobility and low operation voltage of amorphous oxide TFTs: Electronic structure, electron transport, defects and doping, J. Disp. Technol. **5**, 273 (2009).

[46] Kenji Nomura, Hiromichi Ohta, Akihiro Takagi, Toshio Kamiya, Masahiro Hirano, and Hideo Hosono, Room-temperature fabrication of transparent flexible thin-film transistors using amorphous oxide semiconductors, Nature (London) **432**, 488 (2004).

[47] Kyeongmi Lee, Kenji Nomura, Hiroshi Yanagi, Toshio Kamiya, Eiji Ikenaga, Takeharu Sugiyama, Keisuke Kobayashi, and Hideo Hosono, Band alignment of $InGaZnO_4$/Si interface by hard x-ray photoelectron spectroscopy, J. Appl. Phys. **112**, 033713 (2012).

[48] A. de Jamblinne de Meux, Geoffrey Pourtois, Jan Genoe, and Paul Heremans, Comparison of the electronic structure of amorphous versus crystalline indium gallium zinc oxide semiconductor: Structure, tail states and strain effects, J. Phys. D **48**, 435104 (2015).

[49] Jürg Hutter, Marcella Iannuzzi, Florian Schiffmann, and Joost VandeVondele, CP2K: Atomistic simulations of condensed matter systems, Comput. Mol. Sci. **4**, 15 (2014).

[50] Joost VandeVondele, Matthias Krack, Fawzi Mohamed, Michele Parrinello, Thomas Chassaing, and Jürg Hutter, QUICKSTEP: Fast and accurate density functional calculations using a mixed Gaussian and plane waves approach, Comput. Phys. Commun. **167**, 103 (2005).

[51] C. Hartwigsen, Sephen Goedecker, and Jürg Hutter, Relativistic separable dual-space Gaussian pseudopotentials from H to Rn, Phys. Rev. B **58**, 3641 (1998).

[52] S. Goedecker, M. Teter, and J. Hutter, Separable dual-space Gaussian pseudopotentials, Phys. Rev. B **54**, 1703 (1996).

[53] M. Krack, Pseudopotentials for H to Kr optimized for gradient-corrected exchange-correlation functionals, Theor. Chem. Acc. **114**, 145 (2005).

[54] Joost VandeVondele and Jürg Hutter, Gaussian basis sets for accurate calculations on molecular systems in gas and condensed phases, J. Chem. Phys. **127**, 114105 (2007).

[55] Yong Youn, Youngho Kang, and Seungwu Han, An efficient method to generate amorphous structures based on local geometry, Comput. Mater. Sci. **95**, 256 (2014).

[56] Graeme Henkelman and Hannes Jnsson, Improved tangent estimate in the nudged elastic band method for finding minimum energy paths and saddle points, J. Chem. Phys. **113**, 9978 (2000).

[57] Christoph Freysoldt, Blazej Grabowski, Tilmann Hickel, Jörg Neugebauer, Georg Kresse, Anderson Janotti, and Chris G. Van De Walle, First-principles calculations for point defects in solids, Rev. Mod. Phys. **86**, 253 (2014).

[58] A. Alkauskas, P. Dek, J. Neugebauer, A. Pasquarello, and C. G. Van de Walle, *Advanced Calculations for Defects in Materials: Electronic Structure Methods* (Wiley, New York, 2011).

[59] Kenji Nomura, Toshio Kamiya, Hiromichi Ohta, Tomoya Uruga, Masahiro Hirano, and Hideo Hosono, Local coordination structure and electronic structure of the large electron mobility amorphous oxide semiconductor In-Ga-Zn-O: Experiment and *ab initio* calculations, Phys. Rev. B **75**, 035212 (2007).

[60] Deok-Yong Cho, Jaewon Song, Kwang Duk Na, Cheol Seong Hwang, Jong Han Jeong, Jae Kyeong Jeong, and Yeon-Gon Mo, Local structure and conduction mechanism in amorphous In-Ga-Zn-O films, Appl. Phys. Lett. **94**, 112112 (2009).

[61] A. de Jamblinne de Meux, G. Pourtois, J. Genoe, and P. Heremans, Comparison of the electronic structure of amorphous versus crystalline indium gallium zinc oxide semiconductor: Structure, tail states and strain effects, J. Phys. D **48**, 435104 (2015).

[62] We remark that this doping mechanism is different from that used in crystalline material, where a donor state close to the conduction band would provide electrons by thermal excitation.

[63] I. I. Fishchuk, A. Kadashchuk, A. Bhoolokam, A. de Jamblinne de Meux, G. Pourtois, M. M. Gavrilyuk, A. Köhler, H. Bässler, P. Heremans, and J. Genoe, Interplay between hopping and band transport in high-mobility disordered semiconductors at large carrier concentrations: The case of the amorphous oxide InGaZnO, Phys. Rev. B **93**, 195204 (2016).

[64] S. Sallis, K. T. Butler, N. F. Quackenbush, D. S. Williams, M. Junda, D. A. Fischer, J. C. Woicik, N. J. Podraza, B. E. White, A. Walsh, and L. F. J. Piper, Origin of deep subgap states in amorphous indium gallium zinc oxide: Chemically disordered coordination of oxygen, Appl. Phys. Lett. **104**, 232108 (2014).

[65] M. Orita, H. Ohta, M. Hirano, S. Narushima, and H. Hosono, Amorphous transparent conductive oxide $InGaO_3$ $(ZnO)_m (m \leq 4)$: A Zn $4s$ conductor, Philos. Mag. B **81**, 501 (2001).

[66] Arun Suresh, Praveen Gollakota, Patrick Wellenius, Anuj Dhawan, and John F. Muth, Transparent, high mobility InGaZnO thin films deposited by PLD, Thin Solid Films **516**, 1326 (2008).

[67] Kenji Nomura, Toshio Kamiya, and Hideo Hosono, Effects of diffusion of hydrogen and oxygen on electrical properties of amorphous oxide semiconductor, In-Ga-Zn-O, ECS J. Solid State Sci. Technol. **2**, P5 (2012).

[68] Ken Watanabe, Dong Hee Lee, Isao Sakaguchi, Kenji Nomura, Toshio Kamiya, Hajime Haneda, Hideo Hosono, and Naoki Ohashi, Surface reactivity and oxygen migration in amorphous indium-gallium-zinc oxide films annealed in humid atmosphere, Appl. Phys. Lett. **103**, 201904 (2013).

[69] Moon-Seok Kim, Young Hwan Hwang, Sungho Kim, Zheng Guo, Dong-Il Moon, Ji-Min Choi, Myeong-Lok

Seol, Byeong-Soo Bae, and Yang-Kyu Choi, Effects of the oxygen vacancy concentration in InGaZnO-based resistance random access memory, Appl. Phys. Lett. **101**, 243503 (2012).

[70] Hyeon Min Kwon, Myeong Ho Kim, Seung Ryul Lee, Young Bae Kim, and Duck Kyun Choi, Current hysteresis by oxygen vacancy exchange between oxides in Pt/*a*-IGZO/TaO_x/W, Appl. Surf. Sci. **293**, 220 (2014).

[71] Jozeph Park, Chang Sun Kim, Yang Soo Kim, Yun Chang Park, Hyung Jin Park, Byeong-Soo Bae, Jin-Seong Park, and Hyun-Suk Kim, The effect of ITO and Mo electrodes on the properties and stability of In-Ga-Zn-O thin film transistors, J. Electroceram. **36**, 129 (2016).

[72] Joonho Bang, Satoru Matsuishi, and Hideo Hosono, Hydrogen anion and subgap states in amorphous In-Ga-Zn-O thin films for TFT applications, Appl. Phys. Lett. **110**, 232105 (2017).

[73] Shyue Ping Ong, William Davidson Richards, Anubhav Jain, Geoffroy Hautier, Michael Kocher, Shreyas Cholia, Dan Gunter, Vincent L. Chevrier, Kristin A. Persson, and Gerbrand Ceder, PYTHON materials genomics (PYMATGEN): A robust, open-source PYTHON library for materials analysis, Comput. Mater. Sci. **68**, 314 (2013).